RSC Advances

PAPER

View Article Online
View Journal | View Issue

Cite this: *RSC Adv.*, 2015, **5**, 90904

Catalytic conversion of glucose and cellobiose to ethylene glycol over Ni–WO_3/SBA-15 catalysts†

Yueling Cao,[ab] Junwei Wang,*[a] Maoqing Kang[a] and Yulei Zhu[a]

Received 2nd August 2015
Accepted 19th October 2015

DOI: 10.1039/c5ra15400f

www.rsc.org/advances

Hydrogenolysis of glucose and cellobiose, used as the model feedstocks, over Ni–WO_3/SBA-15 catalysts has been investigated to probe the influencing factors for the conversion of cellulose to ethylene glycol (EG). The conversion of glucose and cellobiose to EG showed different dependencies on reaction temperature; a lower reaction temperature was needed for the former. Additionally, the surface atomic ratio of W to Ni on the Ni–WO_3/SBA-15 catalysts was the key factor for the product distribution. Both glucose and cellobiose had their own optimum W–Ni ratio for the production of EG, and the ratio of W to Ni for glucose was slightly lower than that of cellobiose. On the other hand, the Ni–WO_3/SBA-15 catalysts were thoroughly characterized by N_2 adsorption–desorption, X-ray diffraction (XRD), hydrogen-temperature programmed reduction (H_2-TPR), X-ray photoelectron spectroscopy (XPS) and transmission electron microscopy (TEM). The results indicated that the reducibility of Ni–WO_3/SBA-15 catalysts with high Ni loading was more similar to that of pure NiO. More importantly, the change of surface atomic content of Ni and W of Ni–WO_3 catalysts with various Ni loadings resulted from the surface W species of the catalysts being gradually covered by Ni species with the increase of Ni loading.

1. Introduction

Utilization of lignocelluloses, the most abundant non-edible biomass in nature, as a renewable hydrocarbon source will gain importance in the industrial production of liquid fuels and chemical substances for sustainability.[1,2] So far, there have been many studies on the conversion of lignocellulosic materials into glucose, polyol, 5-HMF, organic acids, and gaseous hydrocarbons using various processes.[3–12] Among the various chemical transformation processes of cellulose, the one-pot catalytic transformation of cellulose to ethylene glycol (EG) has attracted considerable attention because EG is widely used in the synthesis of resins, automobile antifreeze, cosmetics, *etc.*[5,13]

Since the first report by Ji *et al.*, on cellulose conversion to EG, much progress has been devoted to in designing effective catalysts and revealing the reaction mechanism.[5,14–22] The process of one-pot conversion of cellulose to EG involves three consecutive reactions: (1) hydrolysis of cellulose to cellooligsaccharides and glucose; (2) retro-aldol condensation of these sugar intermediates to glycolaldehyde; and (3) hydrogenation of glycolaldehyde to EG. Additionally, the retro-aldol condensation and hydrogenation reaction are catalyzed by tungstic compounds and metal Ni or Ru, respectively.[21,22] Thus, the ratio of W to Ru or Ni is proved to be crucial for obtaining high yield of EG.[15,17,20] More importantly, it is believed that the homogeneous H_xWO_3 instead of heterogeneous tungsten species or the partly reduced WO_3 is the real active species to promote the selective cleavage of C–C bond of cellulose to form glycolaldehyde.[17,19]

The production of EG from glucose or cellobiose mainly involves the retro-aldol condensation of glucose or cellobiose to glycolaldehyde and the hydrogenation of glycolaldehyde to EG. Meanwhile, some other reactions, such as hydrogenation of glucose to sorbitol, and isomerization of glucose to mannose and fructose followed by subsequent hydrogenation to mannitol and sorbitol, as illustrated in Scheme 1, can also proceed and will compete with the reaction of retro-aldol condensation. Thus, the main impediment to the selective production of EG from cellulose is that how to match the hydrogenation rate and the formation rate of glycolaldehyde. When the hydrogenation rate is lower than the formation rate of glycolaldehyde, it will lead to merely a small portion of glycolaldehyde hydrogenated to EG. However, when the hydrogenation rate is higher than the formation rate of glycolaldehyde, it will lead to more portion of glucose hydrogenated to sorbitol before it occurring retro-aldol condensation to form glycolaldehyde.

However, despite these advances, there are still a lot of problems needed to be resolved. For example, it is interesting to know whether high EG yield can be obtained under mild reaction conditions. Whether the same ratio of W to Ru or Ni is suitable for conversion of other substrates, such as cellobiose

[a]*Institute of Coal Chemistry, Chinese Academy of Sciences, Taiyuan 030001, PR China. E-mail: wangjw@sxicc.ac.cn; Fax: +86 351 4069680; Tel: +86 351 4069680*

[b]*University of Chinese Academy of Sciences, Beijing 100049, PR China*

† Electronic supplementary information (ESI) available. See DOI: 10.1039/c5ra15400f

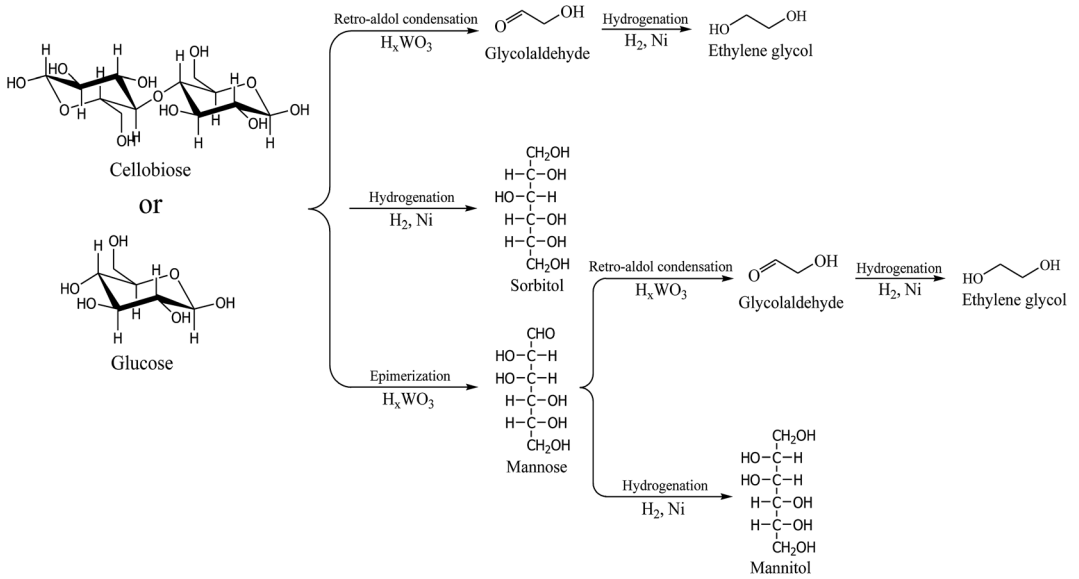

Scheme 1 The reaction path of conversion cellobiose and glucose to ethylene glycol and the main competitive reactions.

and glucose, to EG? Whether the mass transfer effect has an influence on the yield of EG because of many reaction systems adopting the Ru or Ni catalyst combined with one kind of tungstic species.

In our previous work, Ni–WO_3/SBA-15 catalysts showed high activity and selectivity for the one-pot conversion of cellulose to EG.[17] However, the reaction path and mechanism of conversion of cellulose to EG over Ni–WO_3/SBA-15 catalysts were unclear. On the other hand, glucose is the basic unit of cellulose and it is formed as an intermediate in cellulose conversion to EG, while cellobiose is the smallest molecule possessing a β-1,4-glycosidic bond. More importantly, hydrolysis, C–C bond cleavage, and hydrogenation, all the reactions that occur on cellulose conversion, are present on cellobiose conversion. Therefore, the comparison of glucose and cellobiose conversion will provide valuable mechanistic information for the cellulose conversion to EG. In this work the conversion of glucose and cellobiose over Ni–WO_3/SBA-15 catalysts has been systematically studied. High EG yield could be obtained under lower reaction temperatures (<200 °C), and the reaction temperature needed for glucose is lower than that of cellobiose. The products distribution was mainly dependent on the W–Ni ratio of the Ni–WO_3/SBA-15 catalysts. Compared with cellobiose, a slight lower W–Ni ratio for glucose conversion is required to obtain higher EG yield. More importantly, the results from catalyst characterization indicated that the change of W–Ni ratio with Ni loading mainly resulted from that the surface atom content of Ni increased with Ni loading while that of W deceased due to the increasingly Ni gradually covered the active W species.

2. Experimental

2.1 Materials

Glucose (Tianjin Dongliqu Tianda Chemical Reagent Factory, analytic grade), cellobiose (Aladdin Chemistry Co. Ltd, analytic grade), tungstophosphoric acid hydrate [$H_3O_{40}PW_{12}\cdot xH_2O$] (Sinopharm Chemical Reagent Co. Ltd., analytic grade), nickel nitrate hexahydrate [$Ni(NO_3)_2\cdot 6H_2O$] (Sinopharm Chemical Reagent Co. Ltd., analytic grade), and SBA-15 zeolite (Shanghai Novel Chemical Technology Co., Ltd.). All chemicals were used without further purification.

2.2 Preparation of catalysts

All Ni–WO_3/SBA-15 catalysts were prepared by a conventional impregnation method as described previously.[17] Typically, the support, SBA-15, was impregnated with an aqueous solution containing tungstophosphoric acid hydrate [$H_3O_{40}PW_{12}\cdot xH_2O$] and nickel nitrate hexahydrate [$Ni(NO_3)_2\cdot 6H_2O$]. The impregnation volume of metal solution was calculated using the measured incipient wetness of the support. The impregnated catalysts were dried at 100 °C for 12 h and then calcined at 500 °C for 3 h. Before the reaction, all of the catalysts were reduced in a pure hydrogen flow at 500 °C for 1 h. The catalysts are labeled as x% Ni/support, y% WO_3/support or x% Ni–y% WO_3/support, in which x and y stand for the nominal weight loading of metal Ni and WO_3, respectively.

2.3 Catalytic reaction

The catalytic conversion of glucose or cellobiose was performed in a stainless-steel autoclave typically at 6 MPa H_2 (measured at room temperature). For each reaction, glucose or cellobiose (0.5 g), catalyst (0.125 g), and water (40 g) were put in a 100 mL autoclave, which was then purged with hydrogen three times before the reactor was sealed and pressurized with hydrogen (6 MPa). The reaction mixture was heated to a designated temperature with a strong stirring. The zero reaction time was regarded as the time when the temperature reached the set temperature. After the reaction, the autoclave was cooled to room temperature with water bath, and the solid residues were

filtered from the liquid products. The quantification of products was made by an internal standard method.

Compounds with low boiling points, including EG, 1,2-propylene glycol (1,2-PG) and glycerol, were analyzed by a Shimadzu GC-2014 [CBP20 (polar) column (25 × 0.22 mm and 0.25 μm film thickness), flame ionization detector (FID)]. The samples were injected (split ratio: 50) into a CBP20 (polar) column of 25 m × 0.22 mm and 0.25 μm film thickness. The temperature program was as follows: holding at 75 °C for 5.0 min, then increasing from 75 °C to 240 °C at a rate of 30 °C min^{-1}, finally holding at 240 °C for 20 min. Injector and detector temperatures were set as 250 °C and 280 °C, respectively. Compounds with high boiling points, such as glucose, cellobiose, sorbitol and mannitol, were analyzed by an HPLC system [Ca-NP capillary chromatography column, evaporated light scattering detector, water mobile phase, flow rate = 0.6 mL min^{-1}, injection volume = 5.0 μL, T_{column} = 80 °C, $T_{detector}$ = 70 °C].

2.4 Characterization

The N_2 adsorption–desorption isotherms of calcined catalysts were measured at liquid nitrogen temperature (77 K) using a Micromeritics Tristar II (3020). Before the measurements, samples were evacuated overnight at 200 °C and 10^{-2} Pa. Pore size distributions were calculated by analyzing the adsorption branch of the N_2 sorption isotherm using the Barrett–Joyner–Halenda method.

Powder X-ray diffraction (XRD) patterns were obtained by using a Germany Bruker D8 Advance X-ray diffractometer equipped with a graphite monochromator, operating at 40 kV and 40 mA and employing nickel-filtered Cu-Kα radiation (λ = 1.5418 Å).

TPR experiments were carried out in a ChemBet 3000 equipped with a thermal conductivity detector (TCD). For these measurements, 100 mg of sample with a size in the range of 60–80 mesh was placed in a quartz reactor and heated at 450 °C under a N_2 flow of 30 mL min^{-1}, and held at this temperature for 1 h. The reactor was then cooled down to 45 °C and the sample exposed to a steam of 30 mL min^{-1} of 10% H_2/N_2. Subsequently, the sample was heated up to 700 °C at a heating rate of 10 °C min^{-1}.

X-ray photoelectron spectroscopy (XPS) studies were performed with an AXIS ULTRA DLD spectrometer equipped with a hemispherical electron analyzer and an Al Kα (1486.6 eV) X-ray source. Charge referencing was done against adventitious carbon (C 1s at 284.6 eV). The pressure in the analysis chamber was kept lower than 10^{-6} Pa.

Transmission electron microscopy (TEM) experiments were carried out in a JEOL JEM-2100F microscope equipped with an energy dispersive X-ray spectrometer (EDX) operated at 200 kV. The samples were dispersed in ethanol and then placed on a carbon grid before TEM examinations.

3. Results and discussion

3.1 Characterization of Ni–WO_3/SBA-15 catalysts

N_2 adsorption–desorption isotherms for SBA-15 supported Ni–WO_3 catalysts are presented in Fig. 1. All of them were typical for SBA-15 and similar to a Type-IV isotherm according to the IUPAC classification, with a H1 hysteresis loop.[23,24] The shape of the isotherm of pure SBA-15 was preserved even for the catalyst with the highest nickel content, which means that, after the impregnation and subsequent calcinations of nickel and tungsten precursors, the mesoporous nature of the solid was maintained. It should be noted that the nitrogen adsorption isotherms of the Ni–WO_3/SBA-15 catalysts showed a gradual decrease in pore volume and the hysteresis loop became a little broader in the desorption branch with the increase of Ni loading, respectively. These results could be confirmed by physicochemical characterization of Ni–WO_3/SBA-15 catalysts as shown in Table 1. The evaluation of the textural properties of calcined samples from nitrogen adsorption–desorption isotherms at −196 °C revealed that the BET surface area decreased progressively with the loading of nickel, with a drastic reduction for the material with the higher Ni content (Table 1). As shown in Table 1, the BET surface area of 10% Ni–15% WO_3/SBA-15 and 15% Ni–15% WO_3/SBA-15 samples were 301.0 and 279.2 m^2 g^{-1}, respectively, which is much less than that of 3% Ni–15% WO_3/SBA-15 sample (351.5 m^2 g^{-1}). On the other hand, the pore volume of Ni–WO_3/SBA-15 catalysts decreased with the Ni loading and the reduction became more significant with higher loading, which is similar with the trend of the BET surface. Additionally, the average pore diameters of all samples barely changed in comparison with the mesoporous silica, used as support, thus pointing to the presence of nickel

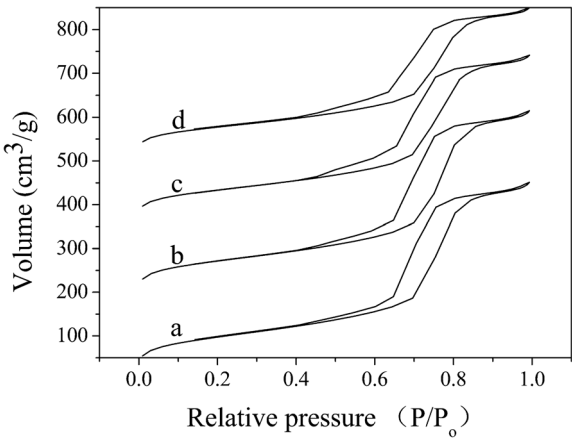

Fig. 1 N_2 adsorption–desorption isotherms: (a) 3% Ni–15% WO_3/SBA-15, (b) 5% Ni–15% WO_3/SBA-15, (c) 10% Ni–15% WO_3/SBA-15, (d) 15% Ni–15% WO_3/SBA-15.

Table 1 Physicochemical characterization of Ni–WO_3/SBA-15 catalysts

Catalysts	S_{BET} (m^2 g^{-1})	V_p (cm^3 g^{-1})	D_{pore} (nm)
3% Ni–15% WO_3/SBA-15	351.5	0.698	7.9
5% Ni–15% WO_3/SBA-15	346.8	0.680	7.8
10% Ni–15% WO_3/SBA-15	301.0	0.605	8.0
15% Ni–15% WO_3/SBA-15	279.2	0.542	7.8

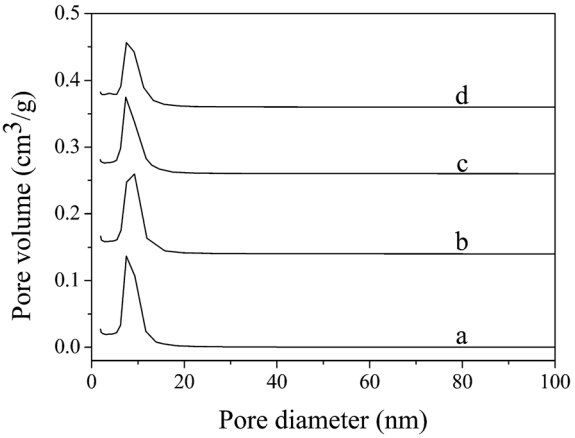

Fig. 2 Pore size distributions of the 3% Ni–15% WO_3/SBA-15 (a), 5% Ni–15% WO_3/SBA-15 (b), 10% Ni–15% WO_3/SBA-15 (c) and 15% Ni–15% WO_3/SBA-15 (d).

oxide and tungsten oxide particles blocking partially the entrance to the mesoporous framework (Fig. 2).

The low-angle powder XRD patterns of the Ni–WO_3/SBA-15 catalysts exhibited a well-resolved diffraction peak, which can be indexed in a hexagonal unit cell as corresponding to the (100) reflection of the SBA-15 silica, confirming that the mesoporous structure was preserved after nickel and tungsten incorporation.[23] However, the presence of nickel and tungsten on the support gave rise to a decrease in the intensity of this low angle peak, which can be explained by the presence of gradual deterioration of the structure with the increase of nickel loading during the calcination procedure. Thus, it could be concluded that the hexagonal arrangement of the SBA-15 frameworks was retained after incorporation of the nickel oxide and tungsten oxide, as could be seen from N_2 adsorption–desorption isotherms and TEM images presented as above and below, respectively.

Typical XRD patterns in the wide-angle region for the samples were shown in Fig. 3B. As shown in Fig. 3B, the characteristic diffraction lines of NiO were clearly visible at 2θ (°) = 37.2, 43.3 62.9, 75.4 and 79.4 (JCPDS 47-1049), excepting for the catalyst with the smallest amount of Ni (3% Ni–15% WO_3/SBA-15), and their intensities, as expected, increased with the Ni loading. It should be noted that the characteristic peaks of WO_3 was not observed regardless of the Ni loading, which indicating that the tungsten oxide were well dispersed in all samples. In addition, these results implied that the nickel oxide was easier to aggregate than the tungsten oxide.

It is well known that reducibility of the nickel species depends on the preparation method, the nature of the support and precursor, as well as the experimental conditions used for the reduction step. Fig. 4 shows the TPR profiles of the calcined Ni–WO_3/SBA-15 catalysts. All samples exhibited only a broad peak, which is due to the co-reduction of NiO and WO_3 was happened during H_2 temperature-programmed reduction procedure as our previous report.[17] It is interesting to note that the initial reduction temperature of samples decreased with Ni loading, from 350 to 300 °C. According our previous report, the

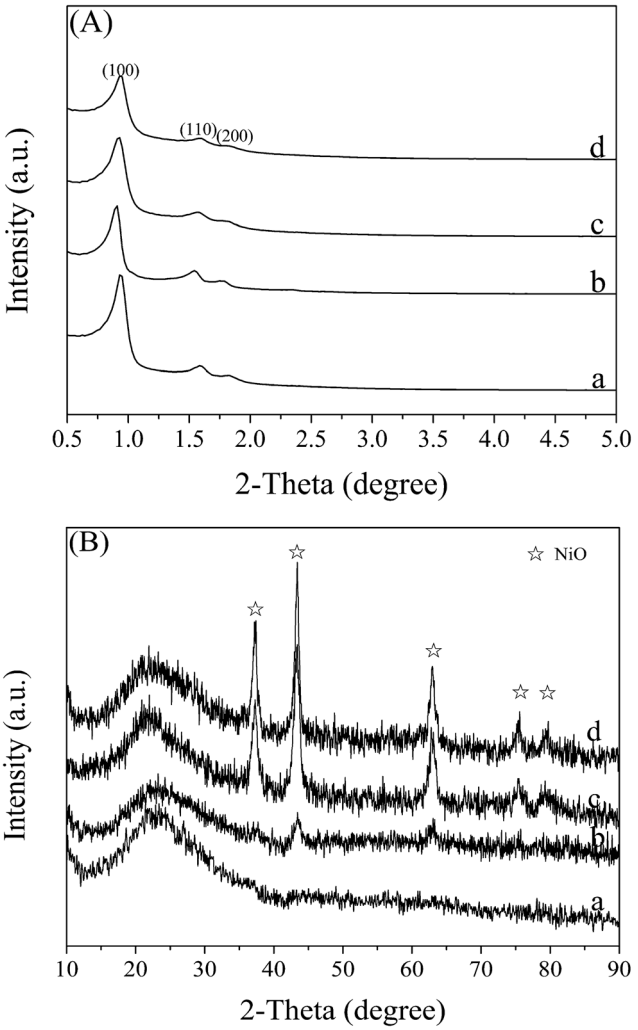

Fig. 3 Low-angle (A) and wide-angle (B) XRD patterns of the 3% Ni–15% WO_3/SBA-15 (a), 5% Ni–15% WO_3/SBA-15 (b), 10% Ni–15% WO_3/SBA-15 (c) and 15% Ni–15% WO_3/SBA-15 (d).

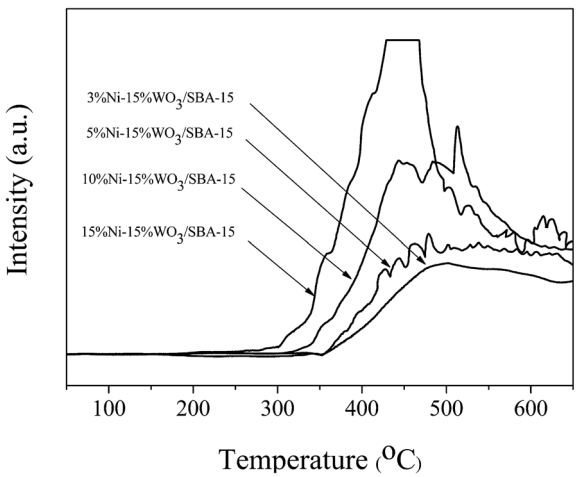

Fig. 4 H_2-TPR patterns of the 3% Ni–15% WO_3/SBA-15 (a), 5% Ni–15% WO_3/SBA-15 (b), 10% Ni–15% WO_3/SBA-15 (c) and 15% Ni–15% WO_3/SBA-15 (d).

Table 2 XPS data of Ni–WO_3/SBA-15 catalysts

Catalysts	Binding energy (eV)		Surface atomic content (at%)				Surface atomic ratio of W/Ni
	Ni $2p_{3/2}$	W $4f_{5/2}$	Ni	W	O	Si	
3% Ni–15% WO_3/SBA-15	855.8	35.4	0.266	0.246	73.052	26.436	0.925
5% Ni–15% WO_3/SBA-15	855.8	35.6	0.488	0.242	77.220	22.050	0.496
10% Ni–15% WO_3/SBA-15	855.7	35.8	0.718	0.192	75.301	27.789	0.267
15% Ni–15% WO_3/SBA-15	855.6	35.8	1.101	0.179	74.320	24.400	0.162

shift to higher temperature resulted from the presence of a strong electronic interaction between NiO and WO_3 for the Ni–WO_3/SBA-15 catalysts.[17] More importantly, the initial reduction temperature of 15% Ni–15% WO_3/SBA-15 sample was same with that of Ni/SBA-15 sample based on our previous result.[17] Thus, it could be concluded that the intensity of interaction between NiO and WO_3 gradually decreased with Ni loading. This might be explained by following reason that the particle size of NiO increased with the Ni loading as shown in XRD results, which making the reduction of NiO was more similar with pure NiO and less proportion of NiO had interaction with WO_3.

Catalysts have been characterized by X-ray photoelectron spectroscopy to obtain more information about the Ni and W oxidation state and the chemical composition of the catalyst surface. The binding energy values of Ni 2p and W 4f along with the relative surface atomic content and the W/Ni atomic ratios of Ni–WO_3/SBA-15 catalysts are presented in Table 2. The bands at 855.6–855.8 eV and at 35.4–35.8 eV are assigned to Ni^{2+} and W^{6+} species, respectively.[25,26] As the Ni loading increased, the binding energy of Ni 2p negatively shifted, which is are in line with H_2-TPR results presented above that the NiO became easier to be reduce with Ni loading. By contrast, the binding energy of W 4f showed the opposite trend, shifting to higher binding energy with the increase of Ni loading, which might result from the interaction between Ni and W decreased with Ni loading as mentioned above. More importantly, as shown in Fig. 5, the Ni 2p signal intensity increased with Ni loading while the W 4f signal intensity exhibited the opposite trend, suggesting that the surface atomic content of Ni and W presented various change trends.

Concerning the surface atom content of the Ni–WO_3/SBA-15 catalysts, as expected, the surface atom content of Ni increased with Ni loading, from 0.266 to 1.101%, which is due to more nickel atoms disperse on the surface of SBA-15. In contrast, the surface atom content of W showed the opposite trend, decreasing with the increase of Ni loading (from 0.246 to 0.179%), although the WO_3 loading was fixed. This might be due to the following reasons. On the one hand, the dispersion of WO_3 decreased with the decrease of surface area of the catalysts as mentioned above. More importantly, the surface active sites of WO_3 were increasingly covered with the surface NiO due to the increase of Ni loading. Concerning the surface W–Ni atomic ratios, their values decreased from 0.925 to 0.162, as expected, with the nickel loading. It should be note that the surface W–Ni atomic ratios of Ni–WO_3 catalysts were a main reason for the product distribution of glucose or cellobiose conversion, which would be presented as below. The low Ni loading means the high W–Ni ratio, which is favorable to form the EG. In contrast, the high Ni loading means the low W–Ni ratio, thus the sorbitol would be the main product if glucose or cellobiose conversion was conducted over the Ni–WO_3 catalysts with high Ni loading.

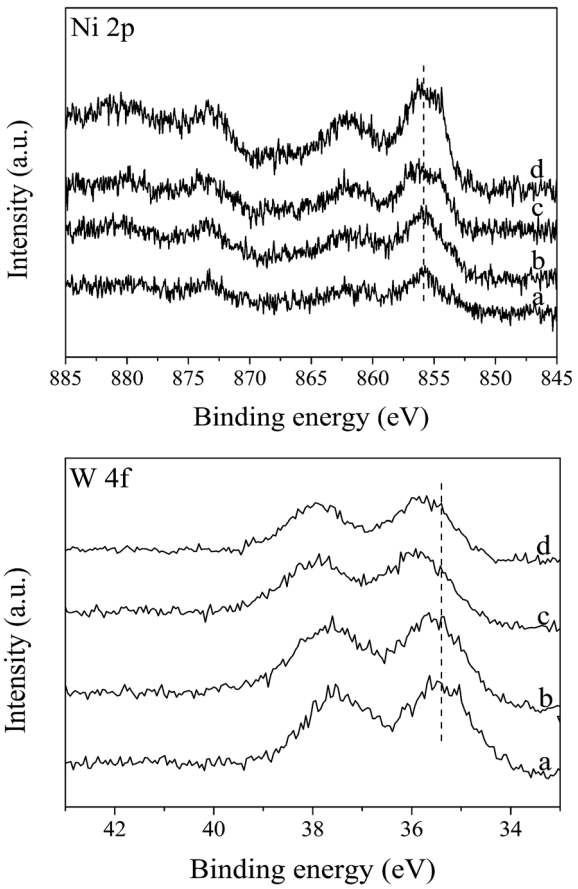

Fig. 5 X-ray photoelectron spectra in the Ni 2p and W 4f regions for the Ni–WO_3/SBA-15 catalysts with different Ni loading: (a) 3% Ni–15% WO_3/SBA-15, (b) 5% Ni–15% WO_3/SBA-15, (c) 10% Ni–15% WO_3/SBA-15, (d) 15% Ni–15% WO_3/SBA-15.

The maintenance of ordered hexagonal arrangement of the SBA-15 frameworks upon nickel and tungsten introduction is further supported by TEM images. As shown in Fig. 6A and C, the Ni–WO_3/SBA-15 samples with different Ni loading showed well-ordered hexagonal arrays of mesopores (1D channels) and unambiguously confirmed that the hexagonal pore structure of the SBA-15 was robust enough to survive the nickel and

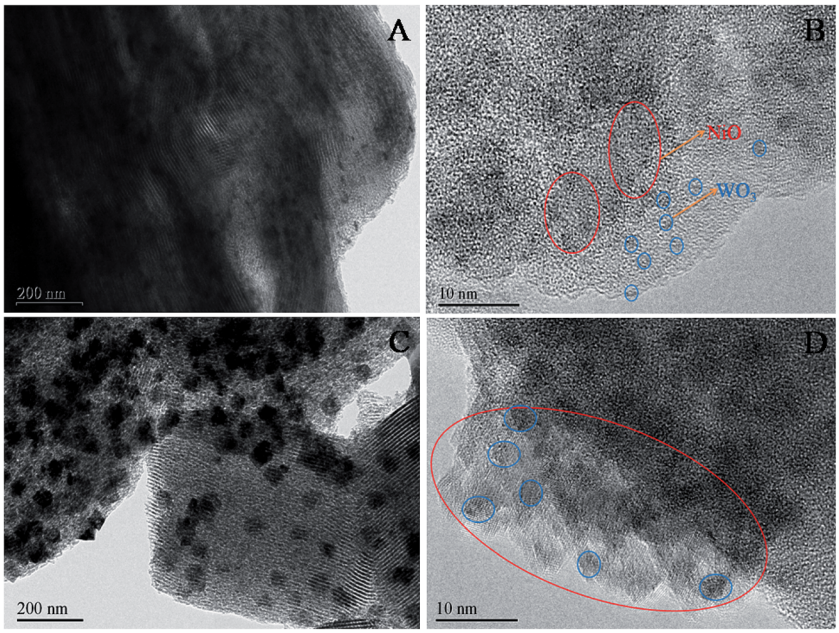

Fig. 6 Representative TEM micrographs of 3% Ni–15% WO_3/SBA-15 (A and B) and 15% Ni–15% WO_3/SAB-15 catalysts (C and D).

tungsten incorporation process. On the other hand, it could be seen from Fig. 6 that the particle sizes of NiO significantly increased with Ni loading, while that of WO_3 only slightly increased. These results were in line with XRD results that the signal intensity of NiO significantly increased with Ni loading, but the characteristic peaks corresponding to WO_3 were not observed regardless of Ni loading. More importantly, as shown in Fig. 6B and D, many WO_3 cluster were exposed on the surface of Ni–WO_3/SBA-15 catalysts when the Ni loading was low (3%). However, part of WO_3 clusters on the catalysts surface was covered by NiO clusters when the Ni loading increased to 15%. These results TEM corroborated the results obtained by XPS analysis that the surface composition of Ni and W exhibited opposite change trends. As mentioned above, the surface ratio of W to Ni was a crucial factor for the products distribution. Thus, the diagram of the influence of surface composition of Ni–WO_3/SBA-15 catalysts with various Ni loading on the products distribution of glucose and cellobiose conversion was presented in Fig. 7.

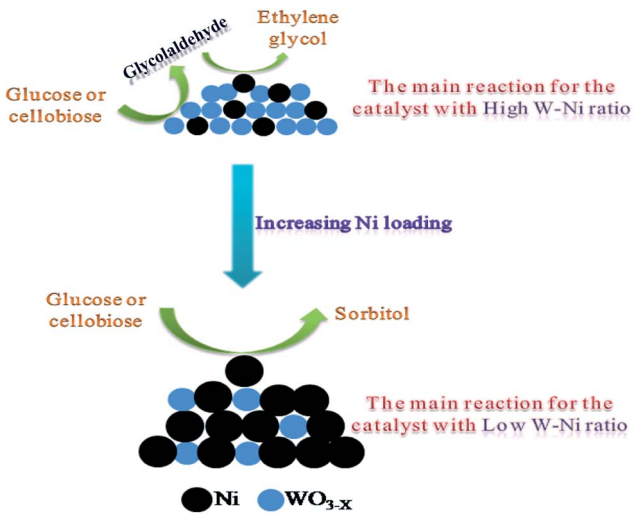

Fig. 7 The influence of surface composition of Ni–WO_3/SBA-15 catalysts with various Ni loading on the products distribution.

3.2 Effect of reaction temperature on glucose and cellobiose conversion

As shown in Scheme 1, the hydrogenation of glucose or cellobiose to form sorbitol and mannitol is competing with their degradation to form glycolaldehyde, which further forms EG *via* catalytic hydrogenation. According to previous report, the reaction selectivity significantly depends on temperatures due to there is a big discrepancy in the activation energies (E_a) between the C–C bond cleavage of glucose (141.3 kJ mol^{-1}) and the hydrogenation of glucose (49.6 kJ mol^{-1}).[21] Therefore, we first conducted reactions at temperatures from 120 °C to 190 °C with 3% Ni–15% WO_3/SBA-15 catalyst.

Tables 3 and 4 illustrates the products distribution from glucose and cellobiose, respectively, at six different temperatures. At a relatively low temperature (120 °C), the cellobiose conversion was only 5.7% while the glucose conversion reached 11.9%, indicating cellobiose had the lower reactivity than that of glucose due to it only possess half of hemiacetal group. It should be noted that trace EG was detected for both glucose and cellobiose conversion, indicating that retro-aldol condensation could occur at this low temperature but at a very low rate. When the reaction of glucose conducted at higher temperatures, both glucose conversion and EG yield increased. The EG yield reached a maximum (32.3%) at 175 °C, and then decreased with increasing reaction temperature. This is due to that both the retro-aldol condensation rate and hydrogenation rate of

Table 3 Effect of reaction temperature on glucose conversion[a]

Reaction temperature (°C)	Reaction time (min)	Conversion (%)	Yield (%)		
			EG	1,2-PG	Glycerol
120	180	11.9	Trace	Trace	0.6
130	180	20.8	3.4	Trace	1.3
145	180	70.4	18.4	0.3	2.5
160	120	96.6	25.5	0.7	3.2
175	80	100	32.3	2.1	3.6
190	30	100	26.3	1.6	2.2

[a] Reaction conditions: glucose 0.5 g, water 40 g, 3% Ni–15% WO_3/SBA-15 0.125 g, H_2 pressure 6 MPa. EG: ethylene glycol, 1,2-PG: 1,2-propylene glycol.

Table 4 Effect of reaction temperature cellobiose conversion[a]

Reaction temperature (°C)	Reaction time (min)	Conversion (%)	Yield (%)		
			EG	1,2-PG	Glycerol
120	180	5.7	Trace	No	No
130	180	16.0	Trace	No	0.7
145	180	46.3	4.5	No	0.9
160	120	83.6	25.5	Trace	1.7
175	80	100	37.3	1.1	2.4
190	30	100	42.4	1.1	2.3

[a] Reaction conditions: cellobiose 0.5 g, water 40 g, 3% Ni–15% WO_3/SBA-15 0.125 g, H_2 pressure 6 MPa. EG: ethylene glycol, 1,2-PG: 1,2-propylene glycol.

glycolaldehyde increased with reaction temperature, but the former was far higher than later, leading to part of glycolaldehyde formed from retro-aldol condensation of glucose occurred side reactions. On the other hand, although cellobiose showed the same trend of its conversion and EG yield, the reaction temperature (190 °C) for obtaining the maximum yield of EG (42.4%) was higher than that of glucose, which resulting from the low reactivity of cellobiose as mentioned above. On the other hand, it should be noted that only trace amount of hexitols was obtained from all range of reaction temperatures which is different with previous report, but high EG yield was obtained at high reaction temperatures.[20] This is due to that the hydrogenation ability of 3% Ni–15% WO_3/SBA-15 catalyst was always insufficient to hydrogenate glucose, but enough to hydrogenate glycolaldehyde because of the activation energy of glycolaldehyde hydrogenation is lower than that of glucose hydrogenation. Zhang *et al.*, reported that the apparent activation energy are 49.6 and 42.6 kJ mol^{-1} for glucose and glycolaldehyde hydrogenation over Ru/C catalysts, respectively.[21]

Comparing the EG yields in the glucose and cellobiose reactions at the same conditions (Fig. 8), it can be found that the former is much faster than the latter in the lower reaction temperatures, suggesting that the retro-aldol condensation of glucose might be much easier than that of cellobiose. However, with the increase of reaction temperature, the EG yield from cellobiose conversion surpassed that from glucose. This is due to that the slow retro-aldol condensation of cellobiose is better matched with the subsequent hydrogenation of glycolaldehyde as previous report.[22] Thus, it can be concluded that a higher reaction temperature is more favorable for the retro-aldol condensation of cellobiose in comparison with that of glucose.

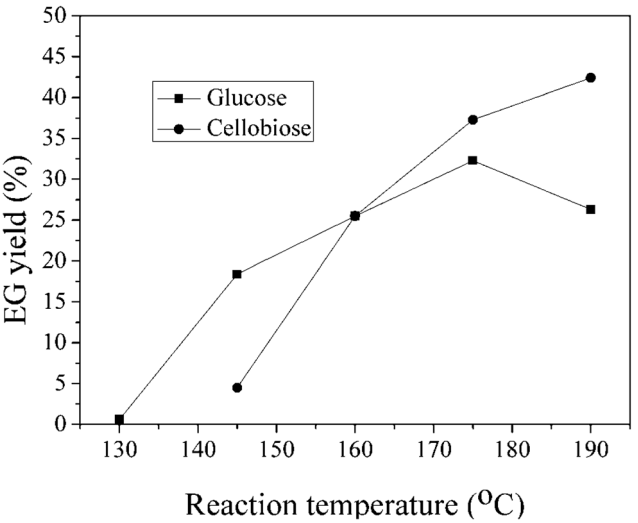

Fig. 8 Ethylene glycol yields as a function of reaction temperature for glucose and cellobiose.

3.3 Effect of W–Ni active sites ratio

As our previous report that 3% Ni–15% WO_3/SAB-15 catalyst possesses the optimum ratio of W to Ni, but this ratio may be not suitable for glucose and cellobiose conversion because the different reactivity between cellulose and these two model

Table 5 Effect of W–Ni active sites ratio on glucose conversion[a]

Catalyst	Conversion (%)	Yield (%)				
		EG	1,2-PG	Glycerol	Sorbitol	Mannitol
3% Ni–15% WO_3/SBA-15	100	32.3	2.1	3.6	Trace	No
5% Ni–15% WO_3/SBA-15	100	41.5	3.6	4.1	4.1	Trace
10% Ni–15% WO_3/SBA-15	100	29.8	2.4	2.9	36.5	7.5
15% Ni–15% WO_3/SBA-15	100	13.5	0.8	2.0	59.7	13.1

[a] Reaction conditions: glucose 0.5 g, water 40 g, catalyst 0.125 g, 175 °C, 80 min, H_2 pressure 6 MPa. EG: ethylene glycol, 1,2-PG: 1,2-propylene glycol.

Table 6 Effect of W–Ni active sites ratio on cellobiose conversion[a]

Catalyst	Conversion (%)	Yield (%)				
		EG	1,2-PG	Glycerol	Sorbitol	Mannitol
3% Ni–15% WO_3/SBA-15	100	42.4	1.1	2.3	Trace	No
5% Ni–15% WO_3/SBA-15	100	42.9	1.8	2.8	4.8	Trace
10% Ni–15% WO_3/SBA-15	100	40.5	3.4	2.8	18.5	2.0
15% Ni–15% WO_3/SBA-15	100	16.3	0.8	2.0	61.5	9.1

[a] Reaction conditions: cellobiose 0.5 g, water 40 g, catalyst 0.125 g, 190 °C, 30 min, H_2 pressure 6 MPa. EG: ethylene glycol, 1,2-PG: 1,2-propylene glycol.

compounds.[17] On the other hand, according to literature, the ratio of W to Ru or Ni active sites proves to be a crucial factor for the products distribution.[15,20] Thus, to explore the best ratio of W to Ni for glucose and cellobiose, the influence of the W–Ni ratio on the EG yield was investigated by changing the Ni loading of Ni–WO_3/SBA-15 catalysts with the WO_3 amount fixed.

As shown in Table 5, the EG yield showed a volcano-shaped curve with the increase of Ni loading. When the Ni loading was low, it was insufficient for the catalytic hydrogenation, leading to merely part of reactive intermediates hydrogenated to EG. However, when the Ni loading is too high, the EG yield decreased but the sorbitol yield increased significantly. On the one hand, this is due to that the hydrogenation rate of glucose increased with the increasing of Ni loading. On the other hand, the Ni covered part active sites of tungsten oxide species, leading to the hydrogenation rate of glucose surpassed the reaction rate of C–C cleavage of glucose. These results are consistent with XPS results that the surface atom content of Ni and W exhibited opposite change trend. To be specific, the relative surface atom content of Ni increased with Ni loading, but that of W decreased with Ni loading due to the part of W was gradually covered by Ni.

Table 6 presents the cellobiose conversion with various ratios of W to Ni. A little unlike the glucose conversion, the EG yield almost remained unchanged at first with the increase of Ni loading. This might be due to that compared with glucose conversion, although the higher ratio of W to Ni of Ni–WO_3/SBA-15 catalyst has the relatively low hydrogenation rate of glycolaldehyde, it is better matched with the slow retro-aldol condensation of cellobiose as mentioned above. When the Ni loading was up to 15%, the direct hydrogenation of cellobiose significantly prevailed over the C–C bond cleavage reaction, leading to the major production of sorbitol and minor production of EG.

4. Conclusion

A series of SBA-15 silica supported Ni–WO_3 catalysts with different Ni loading were prepared for the selective hydrogenolysis of glucose and cellobiose to EG in aqueous solution. Compared with glucose and cellobiose conversion over 3% Ni–15% WO_3/SBA-15 catalysts, higher reaction temperature for cellobiose conversion than that of glucose was needed to obtain the maximum EG yield due to the lower retro-aldol condensation rate of cellobiose compared with that of glucose. The W–Ni ratio was a key factor for the products distribution of glucose and cellobiose conversion. More specially, when the Ni–WO_3/SBA-15 catalyst with lower Ni loading was used, the retro-aldol condensation of glucose or cellobiose to glycolaldehyde and its subsequent hydrogenation would be the main reaction path. However, the direct hydrogenation of glucose or cellobiose would prevail if the catalyst with lower W–Ni ratio was used. Compared with glucose conversion, the lower ratio of W to Ni is more favorable for the conversion of cellobiose to EG. The systematic catalyst characterization indicated that the surface atomic ratio of W to Ni of the Ni–15% WO_3 catalysts decreased with the increase of Ni loading. There are two reasons for this. First, nickel and tungsten oxides became less dispersed with the increasing in Ni loading due to the decrease of the BET surface of the catalysts. More importantly, the surface active sites of tungstic species were gradually covered by the gradually increased nickel oxides.

Acknowledgements

This work was financially supported by a grant from the Major State Basic Research Development Program of China (973 Program) (No. 2012CB215305).

References

1 G. W. Huber, S. Iborra and A. Corma, *Chem. Rev.*, 2006, **106**, 4044–4098.
2 A. Corma, S. Iborra and A. Velty, *Chem. Rev.*, 2007, **107**, 2411–2502.
3 A. Onda, T. Ochi and K. Yanagisawa, *Green Chem.*, 2008, **10**, 1033–1037.
4 A. Fukuoka and P. A. Dhepe, *Angew. Chem., Int. Ed.*, 2006, **45**, 5161–5163.
5 N. Ji, T. Zhang, M. Zheng, A. Wang, H. Wang and J. G. Chen, *Angew. Chem.*, 2008, **120**, 8638–8641.
6 Y. Su, H. M. Brown, X. Huang, X. Zhou, J. E. Amonette and Z. C. Zhang, *Appl. Catal., A*, 2009, **361**, 117–122.
7 I.-J. Kuo, N. Suzuki, Y. Yamauchi and K. C.-W. Wu, *RSC Adv.*, 2013, **3**, 2028–2034.
8 J. Zhang, X. Liu, M. Sun, X. Ma and Y. Han, *ACS Catal.*, 2012, **2**, 1698–1702.
9 D. An, A. Ye, W. Deng, Q. Zhang and Y. Wang, *Chem.–Eur. J.*, 2012, **28**, 2938–2947.
10 J. C. Serrano-Ruiz, D. J. Braden, R. M. West and J. A. Dumesic, *Appl. Catal., B*, 2010, **100**, 184–189.
11 Y. Liu, L. Chen, T. Wang, X. Zhang, J. Long, Q. Zhang and L. Ma, *RSC Adv.*, 2015, **5**, 11649–11657.
12 P. Sirous Rezaei, H. Shafaghat and W. M. A. W. Daud, *RSC Adv.*, 2015, **5**, 65408–65414.
13 H. R. Yue, Y. J. Zhao, X. B. Ma and J. L. Gong, *Chem. Soc. Rev.*, 2012, **41**, 4218–4244.
14 Y. Zhang, A. Wang and T. Zhang, *Chem. Commun.*, 2010, **46**, 862–864.
15 M.-Y. Zheng, A.-Q. Wang, N. Ji, J.-F. Pang, X.-D. Wang and T. Zhang, *ChemSusChem*, 2010, **3**, 63–66.
16 I. G. Baek, S. J. You and E. D. Park, *Bioresour. Technol.*, 2012, **114**, 684–690.
17 Y. Cao, J. Wang, M. Kang and Y. Zhu, *J. Mol. Catal. A: Chem.*, 2014, **381**, 46–53.
18 Y. Liu, C. Luo and H. Liu, *Angew. Chem.*, 2012, **124**, 3303–3307.
19 Z. Tai, J. Zhang, A. Wang, M. Zheng and T. Zhang, *Chem. Commun.*, 2012, **48**, 7052–7054.
20 G. Zhao, M. Zheng, J. Zhang, A. Wang and T. Zhang, *Ind. Eng. Chem. Res.*, 2013, **52**, 9566–9572.
21 J. Zhang, B. Hou, A. Wang, Z. Li, H. Wang and T. Zhang, *AIChE J.*, 2014, **61**, 224–238.
22 J. Zhang, X. Yang, B. Hou, A. Wang, Z. Li, H. Wang and T. Zhang, *Chin. J. Catal.*, 2014, **35**, 1811–1817.
23 D. Zhao, J. Feng, Q. Huo, N. Melosh, G. H. Fredrickson, B. F. Chmelka and G. D. Stuchy, *Science*, 1998, **279**, 548.
24 S. J. Gregg and K. S. W. Sing, *Adsorption Surface Area and Porosity*, Academic Press, New York, 1982.
25 Y. Shen and A. C. Lua, *RSC Adv.*, 2014, **4**, 42159–42167.
26 X. Yang, R. Gao, W.-L. Dai and K. N. Fan, *J. Phys. Chem. C*, 2008, **112**, 3819–3826.

